Ground-Motion Prediction Equation for Small-to-Moderate Events at Short Hypocentral Distances, with Application to Induced-Seismicity Hazards

by Gail M. Atkinson

Abstract   The evaluation of seismic hazard from induced seismicity requires the development of ground-motion prediction equations (GMPEs) that are tuned to the key magnitude–distance range for such applications. I use events of **M** 3–6 at hypocentral distances less than 40 km, drawn from the Next Generation Attenuation-West 2 (NGA-West 2) database, to develop a GMPE that accounts correctly for point-source scaling in both magnitude and distance space for such events. The developed GMPE is in demonstrable agreement with the NGA-West 2 database and with the predictions of a stochastic point-source simulation model. The database is sparse at close distances, implying epistemic uncertainty of as much as a factor of 2 in ground-motion amplitudes within 10 km of the hypocenter. An important conclusion from this study is that the ground-motion amplitudes for moderate induced events could be much larger near the epicenter than predicted by most of the NGA-West 2 GMPEs. The potential for large motions is a consequence of the shallow depth of induced events, which places the earthquake fault only a short distance beneath the epicenter.

Introduction

A pressing concern in engineering seismology is the evaluation of the seismic-hazard implications of induced seismicity from oil and gas activities, including wastewater disposal and, to a lesser extent, hydraulic fracturing. In parts of North America, the rate of moderate events has increased dramatically over the last decade in response to such activity (Ellsworth, 2013), with damaging events as large as moment magnitude (**M**) 5.7 having likely been triggered (Keranen *et al.*, 2013; Sumy *et al.*, 2014). The ground motions from induced events can be of large amplitude, as they occur at shallow depths and may therefore be experienced at very short hypocentral distances. For example, an event of **M** 4.8 on 12 May 2012 that is believed to have been induced by fluid injection in Timpson, Texas, had an epicentral intensity of VII, causing damage; a subsequent nearby event of magnitude m_{bLg} 4.1 produced a peak ground acceleration (PGA) of $62\%g$ and peak ground velocity (PGV) of 22 cm/s at close epicentral distances (Frolich *et al.*, 2014). It is now recognized that the hazard implications of small-to-moderate events at short hypocentral distances merit careful evaluation, for national seismic-hazard mapping (Rubinstein, 2014) and for evaluation of critical facilities (Atkinson, 2014).

A key component of the evaluation of hazard from induced events is the specification of ground-motion prediction equations (GMPEs), characterizing the expected amplitudes as a function of **M** and distance. There is a pressing need to develop GMPEs that are applicable to induced events. The ground-motion database developed by the Next Generation Attenuation-West 2 (NGA-West 2) project (Ancheta *et al.*, 2014) is helpful in this regard, because it includes a good set of small-to-moderate events of appropriate magnitude (**M** < 6) at a wide range of distances. However, the GMPEs developed by the NGA-West 2 project are not necessarily well suited to the evaluation of induced-seismicity hazards because the NGA-West 2 GMPEs were developed to optimize their performance for the moderate-to-large events at typical distances for natural events, which comprise the key hazard contributions in active tectonic settings. Moreover, in form and functionality, they employ a finite-fault distance metric, such as closest distance to the fault (R_{cd}) or its surface projection (R_{JB}). R_{cd} is a calculated parameter in which one finds the closest distance from the rupture plane to the observation point based on the rupture geometry; R_{JB} is similar, but one finds the shortest distance to the surface projection of the rupture plane. For induced events (**M** < 6), the rupture geometry is not generally known. This makes hypocentral distance a more convenient and transparent distance metric. The hypocentral distance (R_{hypo}) is unambiguously defined from the epicentral location and focal depth, without requiring arbitrary assumptions regarding the associated fault surface. Furthermore, use of R_{hypo} allows for a functional form of GMPE that will correctly reflect
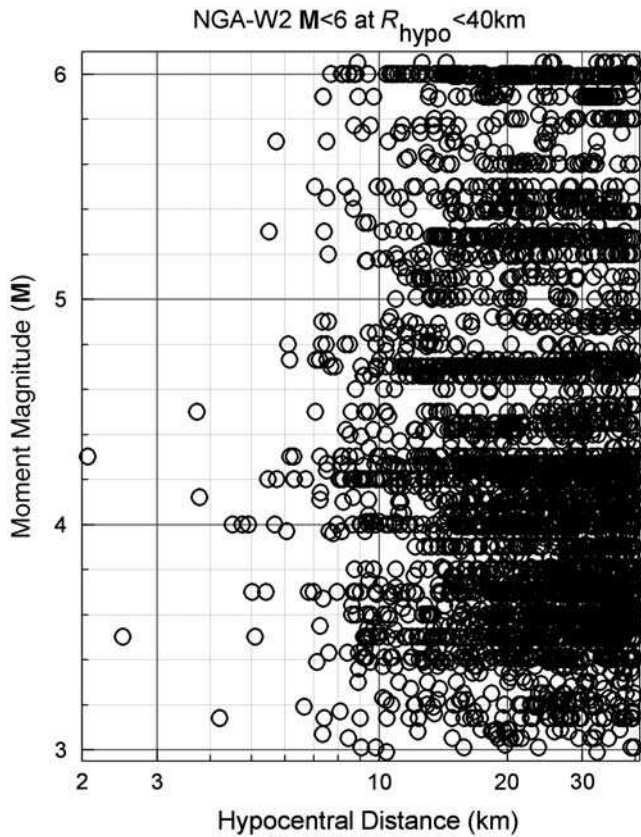
NGA-W2 **M**<6 at R_{hypo} <40km

Figure 1. Distribution of the study database in moment magnitude and hypocentral distance.

the point-source scaling attributes that apply to small-to-moderate events.

In this article, I use the NGA-West 2 database (Ancheta *et al.*, 2014) to develop a preliminary GMPE for events of **M** 3–6 at distances less than 40 km; thus the GMPE is tuned to perform best in the magnitude–distance range that is critical for induced-seismicity applications. The focus on small-to-moderate events allows development of a simple GMPE in R_{hypo} that accounts correctly for point-source scaling in both magnitude and distance space. I make the implicit assumption that the ground motions from induced events will be comparable with those from naturally occurring events of the same magnitude and hypocentral distance, in accord with the inference of Douglas *et al.* (2013). Evidence in support of this assumption is provided by Yenier and Atkinson (unpublished manuscript, 2015; see Data and Resources), who show the stress parameter (which scales high-frequency ground motions) appears to be comparable for natural and induced events when its dependence on focal depth is taken into account. Focal depth is an important factor, as there appears to be a significant increase in stress parameter with increasing depth (Yenier and Atkinson, unpublished manuscript, 2015; see Data and Resources); this may act to limit the stress parameter, and hence high-frequency motions, for induced events. In the future, when richer ground-motion databases from induced events become available, it will be feasible to develop more refined models. At

present, however, available ground-motion data from moderate-induced events at close distances are sparse.

Database and Methodology

The ground-motion database for this study is a subset of the NGA-West 2 database, containing horizontal-component response spectra and peak ground motions for events of **M** 3–6 at $R_{hypo} \leq 40$ km that pass the selection criteria used by Boore *et al.* (2014) in deriving their NGA-West 2 GMPE. The recorded motions are corrected to the equivalent amplitudes for a reference site condition of the B/C boundary (near-surface shear-wave velocity of 760 m/s; this corresponds to soft rock), using the site-amplification factors of Boore *et al.* (2014). Thus, the ground-motion database for the study is the same as that used by Boore *et al.* (2014), and only the focus of the GMPE is different: I focus on small-to-moderate events at close distances, using R_{hypo} as the distance metric. The GMPE will apply to soft-rock site conditions, but the soil response model of Boore *et al.* (2014) may be used to provide a correction to the predicted amplitudes for use with other site conditions.

Figure 1 shows the distribution of the included data in magnitude and distance. This distribution enables a well-constrained empirical regression to characterize amplitudes for **M** 3–6 at R_{hypo} from 10 to 40 km, in which magnitude–distance trade-offs (at $R_{hypo} > 10$ km) should be minimal. At closer distances, the sparseness of the data will lead to uncertainties in the distance–saturation characteristics, which will require careful evaluation and constraint of the functional form, as discussed further below. The included events are entirely from California. However, it has been noted that ground motions for moderate events in eastern North America are not significantly different from those in California at distances < 50 km except at high frequencies (> 5 Hz), and thus the results are likely to be more widely applicable at most frequencies (e.g., Babaie Mahani and Atkinson, 2013).

I begin with a regression of data amplitudes to the simple functional form

$$\log Y = c_0 + c_1 \mathbf{M} + c_2 \mathbf{M}^2 + c_3 \log R, \qquad (1)$$

in which Y is the ground-motion parameter (specifically, the orientation-independent horizontal-component 5% damped pseudospectral acceleration [PSA] at a given frequency, or the PGA, or PGV); logs are in base 10; **M** is moment magnitude; and R is an effective point-source distance that includes near-source distance–saturation effects using an effective depth parameter (see Atkinson and Silva, 2000; Boore, 2009; Yenier and Atkinson, 2014),

$$R = \sqrt{(R_{hypo}^2 + h_{eff}^2)}. \qquad (2)$$

To constrain the near-source behavior, I set

$$h_{eff} = \max(1, 10^{(-1.72 + 0.43 \mathbf{M})}), \qquad (3)$$

Table 1
Summary of Input Parameters for Point-Source Stochastic
Simulations

Input Parameter	Value Used for Simulations
Source model	Brune single-corner spectrum
Stress parameter	$\Delta\sigma = 300$ bars
Geometrical spreading	$R^{-1.3}$ $R \leq 50$ km, $R^{-0.5}$ $R > 50$ km
Effective distance to the equivalent point source	$R = (D^2 + h_{eff}^2)^{0.5}$
Distance-saturation term	$h_{eff} = \max[1, 10^{(-1.72+0.43\mathbf{M})}]$
Quality factor	$Q = \max(170 f^{0.45}, 100)$ (Raoof *et al.*, 1999, adjusted for $\beta = 3.7$)
Crustal amplification	B/C site amplification factors from Atkinson and Boore (2006)
Kappa factor	$\kappa_0 = 0.02$ s
Density	$\rho = 2.8$ g/cc
S-wave velocity (source region)	$\beta = 3.7$ km/s
Ground-motion duration (f_0 from Boore, 2003)	$1/f_0 + 0.05 R_{hypo}$

in which the distance–saturation parameter h_{eff} is as determined by Yenier and Atkinson (2014) from stochastic modeling of a range of global events of $\mathbf{M} \geq 6.0$. Note that a minimum value of $h_{eff} = 1$ km is specified; this is the value from equation (3) when $\mathbf{M}$ 4. The basic idea of the specified GMPE form (equation 1) is that the ground-motion amplitude (in log units), for each selected vibration frequency, will scale up with magnitude, with the quadratic term in $\mathbf{M}$ allowing for a nonuniform scaling as magnitude increases. The amplitude decays linearly with log R, but the use of an effective distance measure for R (equation 2) forces the attenuation curves to saturate (go flat) at near-source distances. The distance–saturation effect is controlled by h_{eff}, with the flattening extending to larger distances as magnitude increases (equation 3). One way to think of this effect is that h_{eff} may represent an average distance down the strike of the fault to the asperity that produces strong ground motion. Because the fault length scales up with magnitude, so too will the value of h_{eff}; for small events with limited fault size (< 1 km), the asperity will necessarily be very close, and thus h_{eff} should be similarly small. By contrast, for large events with a long fault length, the value of h_{eff} may be 10–20 km.

The functional form for the GMPE was chosen as the simplest form likely to be applicable, based on extensive past experience with regression of ground-motion amplitude data. There is significant uncertainty in the minimum-magnitude range of applicability for equation (3), which will map into epistemic uncertainty in the developed GMPE; this will be explored further later. It should be recognized that the functional form is significantly constrained by the explicit definition of the distance-saturation term through equations (2) and (3). I view this as a significant advantage overall, because this term has been defined by a combination of empirical and modeling studies over a range of magnitudes and calibrated within the framework of a point-source stochastic model (Yenier and Atkinson, 2014;

Yenier and Atkinson, unpublished manuscript, 2015, see Data and Resources). Nevertheless, it is a key assumption and an important factor in the differences between the GMPE model proposed here and in the NGA-West 2 GMPEs.

The coefficients of equation (1) are determined using the maximum-likelihood regression method of Joyner and Boore (1993). A maximum-likelihood algorithm (or random effects model) is generally preferred over simple least squares to avoid magnitude–distance trade-offs that can occur in the regression of ground-motion datasets (Joyner and Boore, 1993). Such issues are not severe in this dataset due to its good data coverage over a limited magnitude–distance range, and the constraints that are imposed on the near-distance scaling by the specified functional form. I therefore tested the robustness of regression results by also using simple least squares. The determined GMPE is not sensitive to the choice of maximum likelihood versus least squares; the maximum-likelihood results are shown because they are the preferred solution. The robustness of the results is also demonstrated by an evaluation of residuals and by comparison of the results with the predictions of an equivalent point-source stochastic model.

A point-source stochastic model is a particularly effective tool for interpretation of the implied source and path effects of the small-to-moderate event database, due to their limited fault size. The point-source stochastic model treats ground motions as finite-duration band-limited Gaussian noise for which the underlying amplitude spectrum is given by a simple seismological model of source and attenuation processes (Boore, 2003); the motion is assumed to emanate from a single point at a specified distance. The approach is easy to implement, partly due to the availability of the widely cited Stochastic-Method SIMulation (SMSIM) algorithm developed by Boore (2000, 2003). Despite its simplicity, the stochastic point-source model has been remarkably successful at reproducing average ground-motion amplitudes over a wide range of magnitudes, distances, and frequencies (e.g., Boore, 2003; Yenier and Atkinson, 2014; Yenier and Atkinson, unpublished manuscript, 2015, see Data and Resources). In this study, I use time-domain ground-motion simulations generated with the SMSIM program (Boore, 2000, 2003), adopting the western North America (WNA) stochastic ground-motion model parameters of Atkinson *et al.* (2014); the only modification made to the parameters given in Atkinson *et al.* (2014) is that I include an appropriate crustal amplification function so that the predicted motions will be for the horizontal component on B/C conditions (see Table 1). The key source parameters are the seismic moment and stress parameter, whereas path effects are specified by an attenuation model that describes the average effects of geometric spreading and anelastic attenuation (in which anelastic attenuation is inversely proportional to regional quality factor, Q). Table 1 provides the input parameters used for the simulations (as modified from Atkinson *et al.*, 2014). Note the geometric spreading coefficient, which controls the decay of amplitudes with distance, has a value of -1.3 (for $R_{hypo} \leq 40$ km); this value is consistent with attenuation models for WNA (Atkinson *et al.*, 2014; Yenier and Atkinson,

Table 2
Coefficients of Equation (1)

PSA at Frequency	c_0	c_1	c_2	c_3	σ-intra	σ-inter	σ-total
0.2	−4.321	1.080	0.009376	−1.378	0.25	0.18	0.31
0.33	−3.827	1.060	0.009086	−1.398	0.24	0.22	0.32
0.5	−4.462	1.485	−0.03815	−1.361	0.24	0.23	0.33
1	−4.081	1.742	−0.07381	−1.481	0.26	0.22	0.34
2	−3.873	2.060	−0.1212	−1.544	0.29	0.20	0.35
3.33	−2.794	1.852	−0.1078	−1.608	0.30	0.19	0.36
5	−2.266	1.785	−0.1061	−1.657	0.30	0.21	0.37
10	−1.954	1.830	−0.1185	−1.774	0.29	0.25	0.39
20	−2.018	1.826	−0.1192	−1.831	0.28	0.30	0.41
33	−2.283	1.842	−0.1189	−1.785	0.28	0.27	0.39
PGA	−2.376	1.818	−0.1153	−1.752	0.28	0.24	0.37
PGV	−4.151	1.762	−0.09509	−1.669	0.27	0.19	0.33

Equation (1) predicts 5% damped horizontal-component pseudospectral acceleration (PSA, in cm/s^2) for B/C site conditions, peak ground acceleration (PGA, in cm/s^2), and peak ground velocity (PGV, in cm/s). The standard deviation of residuals (σ-total) and its intraevent and interevent components are also given.

2014), eastern North America (ENA; Atkinson and Boore, 2014), and Australia (Allen *et al.*, 2007). It is also consistent with previous work by Atkinson and Morrison (2009), who found that amplitudes from small-to-moderate events attenuate steeply at close distances and at a similar rate in both ENA and WNA. At the distance range considered, the effects of anelastic attenuation, which tend to introduce a frequency-dependent curvature to the decay of log amplitudes with distance, are limited. Note the point-source simulation model provides ground-motion predictions that are expected to be applicable to both ENA and WNA, for frequencies up to 5 Hz.

At higher frequencies (> 5 Hz), the motions for ENA could be larger in amplitude than those simulated here, because I assume a stress parameter that is appropriate for WNA for the assigned geometric spreading and calibration approach (following Yenier and Atkinson, 2014). By contrast, ENA events would generally be expected to have a stress parameter that is on average higher by about a factor of 2 (e.g., Atkinson and Hanks, 1995; Babaie Mahani and Atkinson, 2013). On the other hand, preliminary studies suggest that induced events in Oklahoma have relatively low stress parameters, with the lower stress parameter being related to shallow focal depth (Yenier and Atkinson, unpublished manuscript, 2015, see Data and Resources). Overall, the average stress parameter for induced events is not well known at this time due to a lack of data, and future studies may suggest values that are either higher or lower than the typical WNA value assumed here. The limited current information on the source parameters of induced events maps into epistemic uncertainty in the GMPE that is most pronounced at larger magnitudes and higher frequencies. This is because ground motions are insensitive to stress parameter at frequencies below the spectral corner frequency, which is relatively high for small-to-moderate events.

Results

Table 2 gives the values of the determined coefficients (in cgs units) for equation (1), along with the standard deviation of residuals (σ), subdivided into interevent and intraevent components of variability. The variability is a measure of how much scatter exists in observed amplitudes about the predicted median and is an important consideration in hazard assessment. The intraevent component describes the amplitude variability for a single event (for different sites at a fixed distance), whereas the interevent component reflects the fact that some events have systematically high amplitudes relative to average and others have systematically low amplitudes.

Figure 2 provides an overview-level illustration of the ground-motion amplitudes in comparison with the GMPE for PGA, over the range of magnitudes and distances. The attenuation follows a simple near-linear trend, with the exception of larger magnitudes at $R_{hypo} < 10$ km, for which the effective focal depth term (equation 2) becomes important and controls the distance–saturation effects in the empirical regression. The data appear to be consistent with the assumed model. The lack of saturation in the 2–10 km distance range is the reason that moderate-induced events may be potentially damaging. For example, we may consider PGA > 50 cm/s^2 as the lower-bound threshold for potential damage; this would correspond to modified mercalli intensity VI, based on the correlations of Worden *et al.* (2012). Note that for events with a focal depth of 10 km (an average depth for natural events), we would not generally expect damage for events of $\mathbf{M} < 5$, because the hypocentral distance from the source would exceed 10 km. By contrast, for induced events, typically at depths of 5 km or less, we may exceed 50 cm/s^2 for events of $\mathbf{M} > 3.5$ at short epicentral distances. The potential for strong shaking from small events arises because induced events are close to the surface, bringing the earthquake source very close to the epicenter. The actual damage potential of large-amplitude short-duration events is an important earthquake engineering topic requiring further study but is beyond the scope of this article.

Figure 3 is a plot of the residuals, defined as the difference (in log units) between the observed and predicted
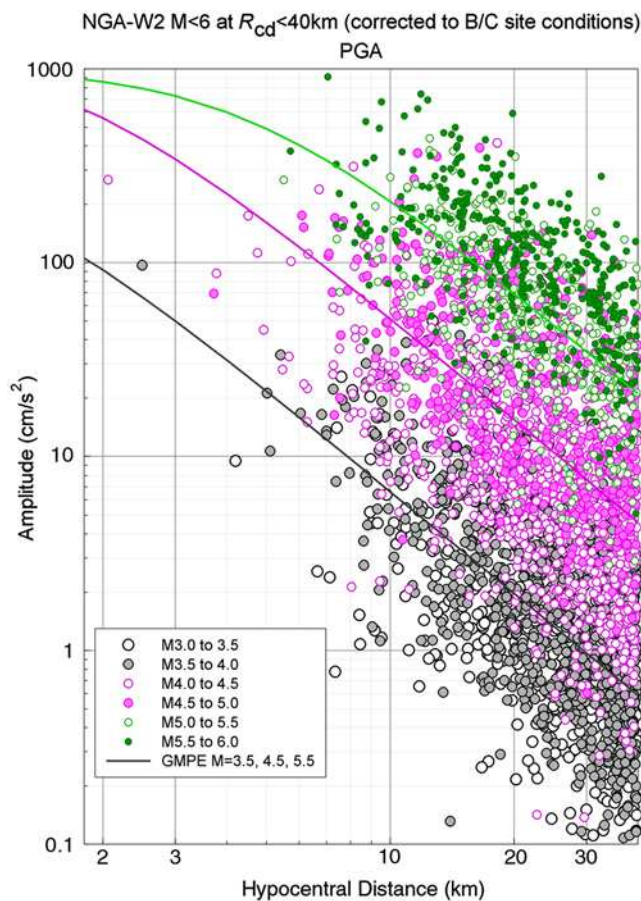
Figure 2. Regression results for peak ground acceleration (PGA). The lines show the ground-motion prediction equation (GMPE) for **M** 3.5, 4.5, and 5.5. The circles show PGA values used in the regression (corrected to B/C site conditions), shaded and sized by magnitude. The color version of this figure is available only in the electronic edition.

Figure 3. PGA residuals (log[observed/predicted]) versus hypocentral distance for regression to equation (1), shown for **M** 3.5–4.5 (large dots) and **M** 4.5–5.5 (small dots). The squares with error bars show the means and standard deviations of residuals in four distance bins (0–10, 10–20, 20–30, and 30–40 km). The color version of this figure is available only in the electronic edition.

motions. The plot suggests the GMPE performs well; there are no residual trends in distance over the primary magnitude range of interest, from **M** 3.5 to 5.5. Mean residuals are near zero over all distances and magnitudes, with standard deviations of ∼0.3–0.4 units (similar to the Boore *et al.*, 2014, standard deviations for small events). The lack of trends in the residuals suggests that further refinements in the functional form of the GMPE are not required.

In Figures 4 and 5, I examine the behavior of the data at 1 and 5 Hz, respectively, for events of **M** 4–6, in comparison with the GMPE. The predictions of the point-source simulation model (obtained from SMSIM with the parameters of Table 1) are shown to provide an interpretation framework. The NGA-West 2 GMPE of Boore *et al.* (2014) is also shown for reference; to plot this in hypocentral distance, it is assumed that for small events $R_{hypo} \approx \sqrt{(R_{JB}^2 + 9^2)}$, in which 9 km is the average focal depth for the included data and R_{JB} is the distance to the surface projection of the fault (Joyner–Boore distance). Essentially, this means we assume the fault is small enough so that the epicentral distance is about the
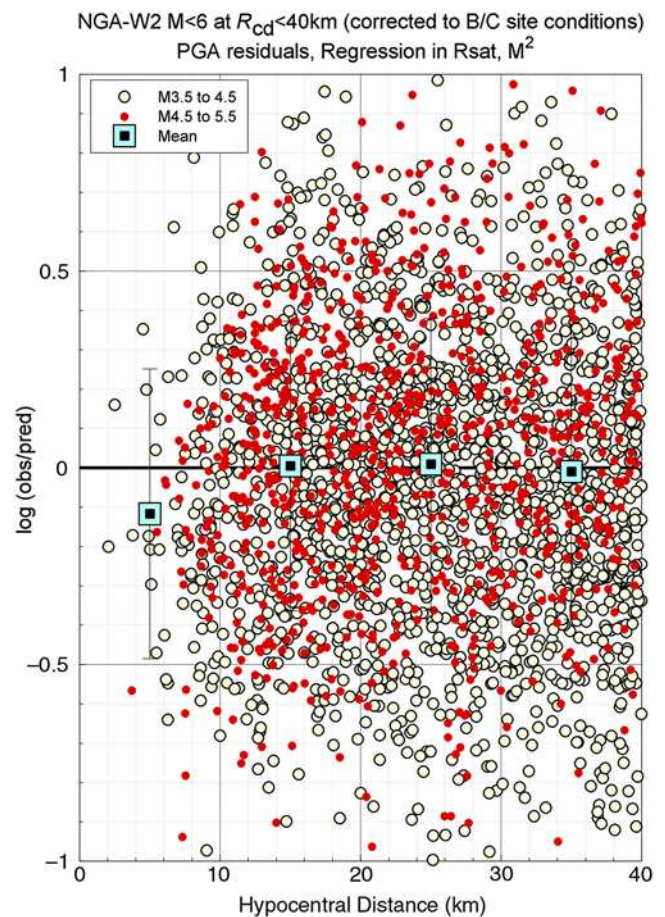
same as the distance to the surface projection of the fault. The effective depth parameter of Yenier and Atkinson (2014), which is indicated on the figures for each magnitude level, controls the near-distance saturation behavior (the rolling-in of the slope). This is why the shape of the simulations and the GMPE agree so well with each other at short distances, for which there are few data. The GMPE agrees well with both the data and the expectations of the point-source simulation model, suggesting the model parameters of Table 1 are providing a good description of the observed amplitudes. A constant offset between the simulations and the GMPE of about 0.1 log units is observed at 1 Hz, possibly reflecting the average influence in the database of unmodeled basin effects in the data (such effects are not included in the simulations).

The effective depth parameter (equation 3) is constrained by the data analyses of Yenier and Atkinson (2014) for events of **M** ≥ 6, but its extension to events as small as **M** 4 (where it attains the minimum assigned value of 1 km) is poorly constrained due to the paucity of data. By inspection of Figures 4 and 5, one may infer the minimum value of $h_{eff} = 1$ at **M** 4

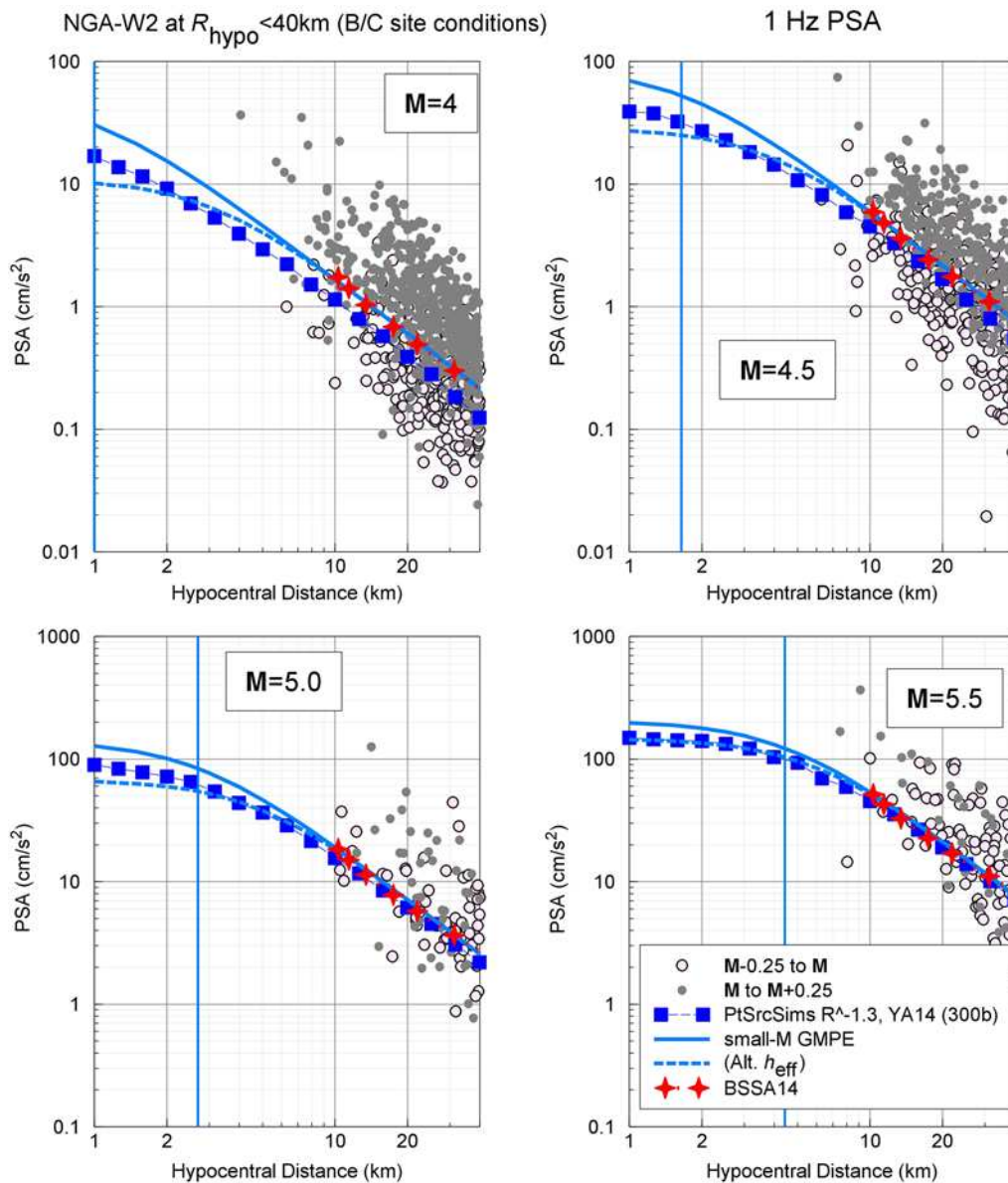**Figure 4.** Comparison of 1 Hz pseudospectral acceleration (PSA) observations for events of **M** 4.0 (±0.25), **M** 4.5 (±0.25), **M** 5.0 (±0.25), and **M** 5.5 (±0.25) with proposed GMPE (solid line) and point-source simulations (squares); both of these use h_{eff} of Yenier and Atkinson (2014; referred to as YA14), in which the h_{eff} value at each magnitude is shown by a vertical line. The effect of an alternative value of h_{eff} on the GMPE, which would increase h_{eff} by a factor of 3 at **M** 4, is shown by the dashed line. The stars show the GMPE predictions of Boore *et al.* (2014, referred as BSSA14). The color version of this figure is available only in the electronic edition.

might be increased by as much as a factor of 3 (i.e., stronger distance–saturation effects) without significantly impacting the goodness of fit. Thus, I postulate an alternative function of $h_{eff} = \max(1, 10^{(-0.28+0.19\,\mathbf{M})})$, which has a value of $h_{eff} = 3$ km at **M** 4, increasing to match the value of $h_{eff} = 7.2$ km at **M** 6 that is given by the Yenier and Atkinson (2014) expression (equation 3). Note that this would imply the expression for h_{eff} comprises two line segments, with a steeper slope for the distance–saturation behavior at **M** > 6; the minimum assigned value of 1 km would be attained at **M** 1.5 under this alternative model. I repeat the regression analysis at two selected frequencies (1 and 5 Hz) for this alternative def-

inition of h_{eff} and show the results in Figures 4 and 5. There is a very faint suggestion in the data at **M** 4 that the adopted model of Yenier and Atkinson (2014) is preferred, but this is not conclusive because the data are sparse.

Figure 6 more closely shows the data constraints on the attenuation behavior in the 0–10 km distance range, comparing 1 Hz residuals over all magnitudes (**M** 3–6) for the two alternative models for the distance–saturation term (h_{eff}). Both models have near-zero mean residual over this distance range. The adopted Yenier and Atkinson (2014) model of h_{eff} appears to be slightly preferred to the alternative model, based on the modest apparent positive residual (observations larger
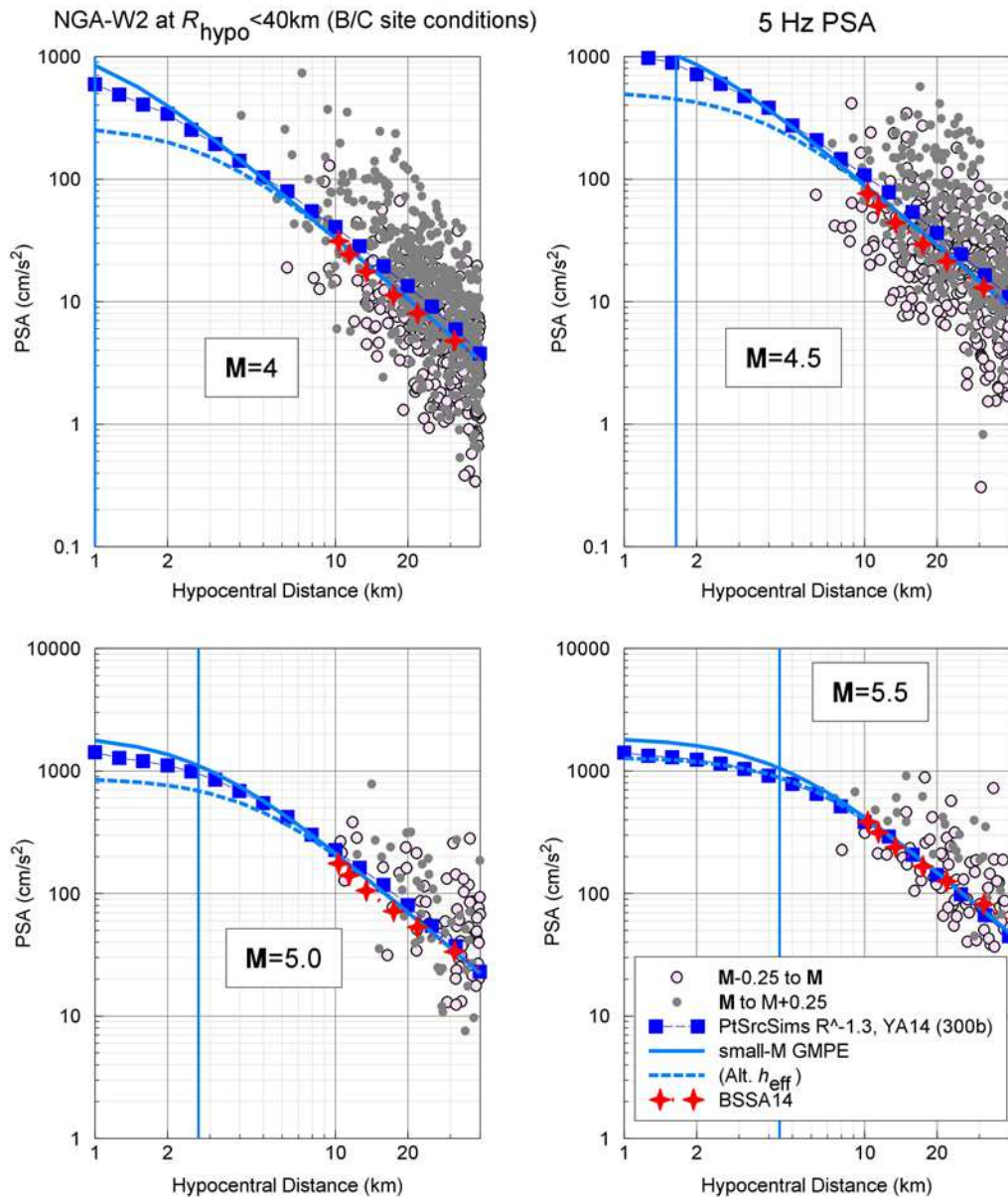
Figure 5. Comparison of 5 Hz PSA observations for events of **M** 4.0 (±0.25), **M** 4.5 (±0.25), **M** 5.0 (±0.25), and **M** 5.5 (±0.25) with proposed GMPE (solid line) and point-source simulations (squares); both of these use h_{eff} of Yenier and Atkinson (2014; referred to as YA14), in which the h_{eff} value at each magnitude is shown by a vertical line. The effect of an alternative value of h_{eff} on the GMPE, which would increase h_{eff} by a factor of 3 at **M** 4, is shown by the dashed line. The stars show the GMPE prediction of Boore *et al.* (2014, referred as BSSA14). The color version of this figure is available only in the electronic edition.

than predicted) for the latter model for both of the closest distance bins. However, the data are too sparse to draw meaningful conclusions. The plot is shown for 1 Hz; other frequencies are similar in their behavior. On balance, the adopted Yenier and Atkinson (2014) form for the distance–saturation term is reasonable, though it might be increased for small events by as much as a factor of 3 and still be relatively consistent with the data. On the other hand, the saturation distances could also be decreased by a similar amount without impacting the fit. This implies an epistemic uncertainty of as much as a factor of 2 in PSA amplitudes at close hypocentral distances (3–5 km). In other words, the average predicted motions for events of

M ∼ 4 near the source might be either higher or lower than those predicted by the GMPE, by a factor of 2.

Discussion and Conclusions

An empirical GMPE that is tuned for the modeling of ground-motion amplitudes from small-to-moderate events (**M** ≤6) at close distances (R_{hypo} ≤ 40 km) has been developed. This model is in demonstrable agreement with the NGA-West 2 database over its applicable magnitude–distance range (in Fig. 1, generally **M** 3–6 at R_{hypo} > 5 km); it is also consistent with the predictions of a stochastic point-source simulation model.
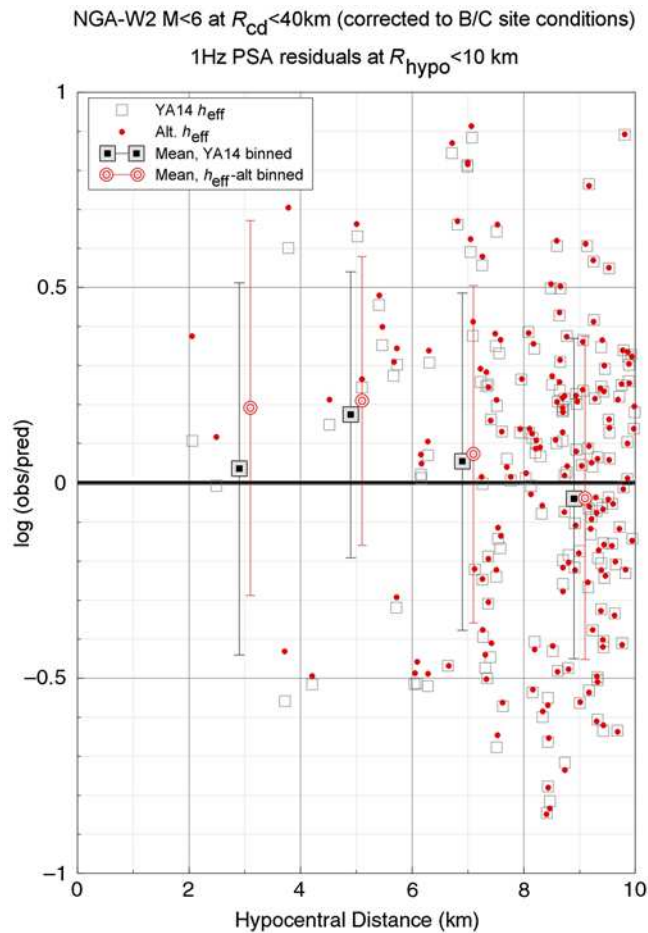
Figure 6. 1 Hz residuals for GMPE within 10 km for Yenier and Atkinson (2014) h_{eff} model (squares; referred to as YA14) and for alternative h_{eff} model with lesser distance saturation (circles). Symbols with error bars are the means and standard errors of data points in hypocentral distance range 2–4, 4–6, 6–8, 8–10 km. The color version of this figure is available only in the electronic edition.

However, the database is sparse at very close distances, implying an epistemic uncertainty of about a factor of 2 in ground-motion amplitudes at very close distances ($R_{hypo} < 10$ km). Resolving this uncertainty will require further analysis with improved short-distance datasets. It is also important to evaluate the applicability of the model to induced events. This research is currently underway.

The results of this study can be compared with those of Douglas *et al.* (2013), who used small-magnitude data from induced events, along with stochastic simulations, to develop a GMPE for induced earthquake ground motions in geothermal areas, including several areas in Europe and California. Their database contains smaller magnitudes ($\mathbf{M} < 4.5$) than are used in this study but has the advantage of including closer distances. Douglas *et al.* also chose to use hypocentral distance as the distance metric and corrected all ground motions to a reference rock condition (about 1100 m/s, slightly stiffer than that used in this study). In Figure 7, I compare the 5 Hz PSA data from the Douglas *et al.* (2013) dataset with the GMPE developed in this study, for magnitudes of 2.5–4.0;

the Douglas *et al.* empirical GMPE is also shown for comparison. Several interesting observations are apparent. Most importantly, the data from the Douglas *et al.* study are in good agreement with the NGA-West 2 data in the region of overlap and with the GMPE developed here. This agreement supports the view of Douglas *et al.* (2013) that the ground-motion amplitudes of natural and induced events are generally indistinguishable. Moreover, the comparison supports the steep scaling of amplitudes with distance ($1/R^{1.3}$) used in the stochastic model for this study. The GMPE proposed here has a noticeably steeper slope than that of Douglas *et al.* (2013). This is because of their choice of functional form, which results in a flatter slope, more nearly in accord with the assumed $1/R$ geometric spreading used in their stochastic simulations. Consequently, the GMPE of this study predicts much higher amplitudes at very close distances. This highlights the importance of geometric spreading in determining maximum ground-motions from small-magnitude events, for which distance–saturation effects may be minimal.

An important conclusion from this study is that both point-source modeling and empirical data suggest the ground-motion amplitudes for moderate events could be quite large if they occur at shallow depth. At near-epicentral distances, the amplitudes exceed those predicted by most of the NGA-West 2 GMPEs. The effect is particularly pronounced for the GMPE of Boore *et al.* (2014), due to their use of R_{JB} as the distance metric. This is illustrated in Figure 8, which shows the effect of focal depth on PSA at 1 and 5 Hz, when plotted in terms of epicentral distance. For the NGA-West 2 records used in this study, the average focal depth is 9 km. If we assume $R_{JB} \approx$ epicentral distance, we observe the small-$\mathbf{M}$ GMPE of this study agrees well with the NGA-West 2 GMPE of Boore *et al.* (2014), if a focal depth of 9 km is assigned when converting from hypocentral to epicentral distance. However, if the actual focal depth is only 2 km, the predicted amplitudes are larger by about a factor of 4 for small events ($\mathbf{M}$ 4.5) directly above the earthquake, in comparison with the Boore *et al.* (2014) GMPE; at larger magnitudes ($\mathbf{M}$ 6), the stronger distance–saturation diminishes this effect, making focal depth less important.

The model proposed here agrees more closely with the NGA-West 2 GMPEs of Abrahamson *et al.* (2014), Campbell and Bozorgnia (2014), and Chiou and Youngs (2014), because these authors all used distance metrics such as R_{cd}, which implicitly include the influence of depth. However, in general, the NGA-West 2 GMPEs have a tendency to predict lower near-distance amplitudes for an $\mathbf{M}$ 4.5 event than the point-source model described herein would predict. This stems from the combination of the regression focus and the choice of functional form for suitability for larger events, as well as being influenced in some cases by the use of a finite-fault distance metric. An exception is the NGA-West 2 GMPE of Abrahamson *et al.* (2014), which predicts amplitudes that equal or exceed those suggested by this study over the entire range plotted in Figure 8. In fact, the high end of all of the
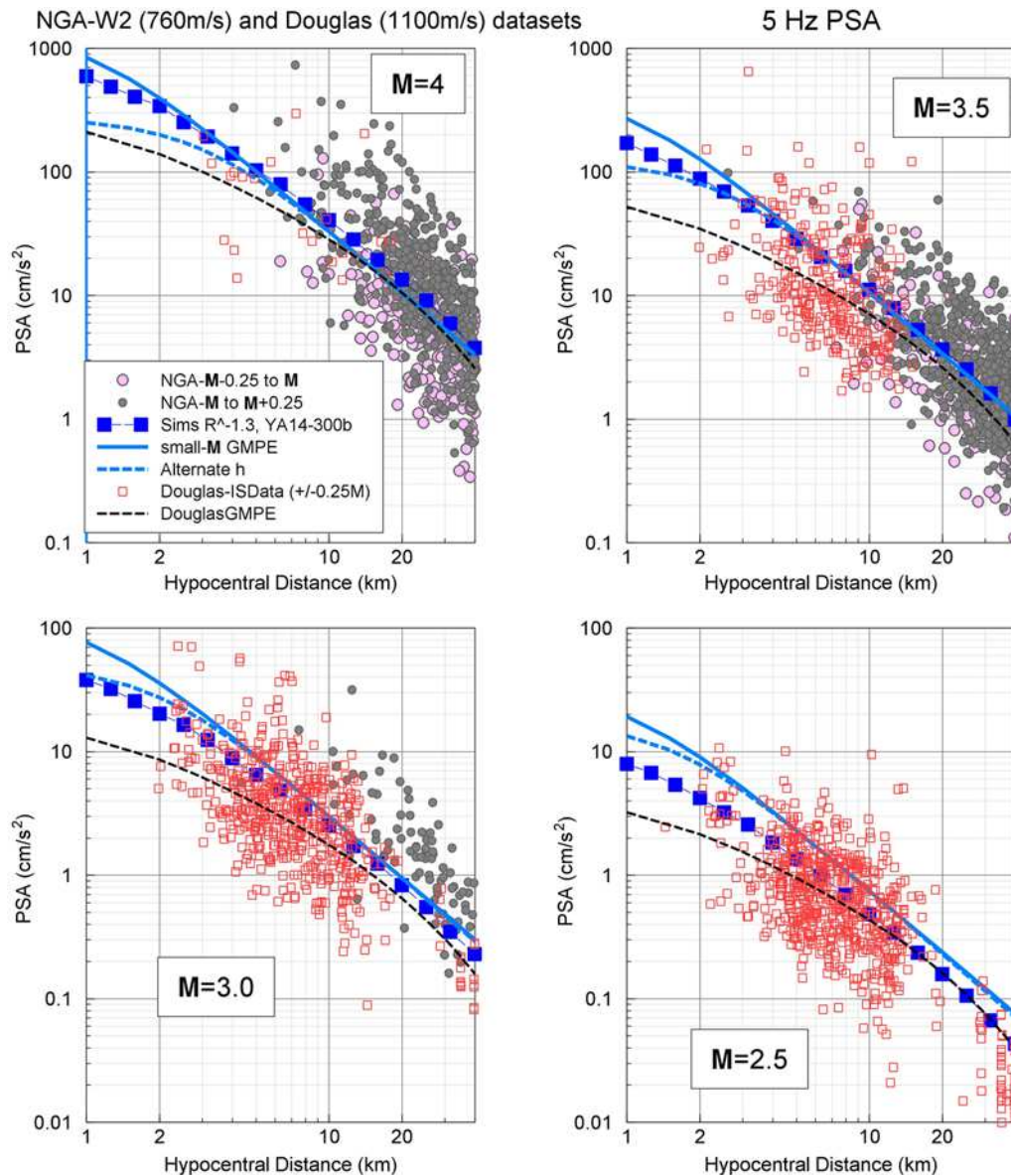
Figure 7. Comparison of 5 Hz PSA observations for events of **M** 4.0 (±0.25), **M** 3.5 (±0.25), **M** 3.0 (±0.25), and **M** 2.5 (±0.25) with proposed GMPE (solid line) and point-source simulations (squares); both use the h_{eff} of Yenier and Atkinson (2014; referred to as YA14), in which the h_{eff} value at each magnitude is shown by a vertical line. The effect of an alternative value of h_{eff} on the GMPE, which would increase h_{eff} by a factor of 3 at **M** 4, is shown by the dashed line. The circles are the NGA-West 2 data, and squares are data of Douglas *et al.* (2013). The light dashed line is the GMPE proposed by Douglas *et al.* The color version of this figure is available only in the electronic edition.

amplitude bars for the NGA-West 2 models in Figure 8 comes from the Abrahamson *et al.* (2014) GMPE.

A key reason for the difference between the predictions of this GMPE and those of the alternative NGA-West 2 models lies in the specification of the distance-saturation model through the h_{eff} term in the functional form. This choice was motivated (and calibrated) for this study using empirical and modeling studies as described by Yenier and Atkinson, (2014) and Yenier and Atkinson (unpublished manuscript, 2015; see Data and Resources) over a broad magnitude range. By comparison, each of the NGA-West2 models takes a different approach to distance saturation effects: each is

largely optimized to fit the near data from larger events. For example, Chiou and Youngs (2014) use an effective depth term that is similar in concept to that employed here, but which imposes a relatively large effective depth (7 km) for events of **M** 3–4; it is noteworthy that this term was calibrated only for events of **M** > 6, because they were not primarily concerned with the smaller events. In contrast, the Abrahamson *et al.* (2014) model specifically reduced the effective depth term for smaller-magnitude events to improve the magnitude range of its applicability. They introduce a break in the magnitude scaling for events of **M** < 5 and impose a value of $h_{eff} = 1$ km at **M** 4 (similar to this study).
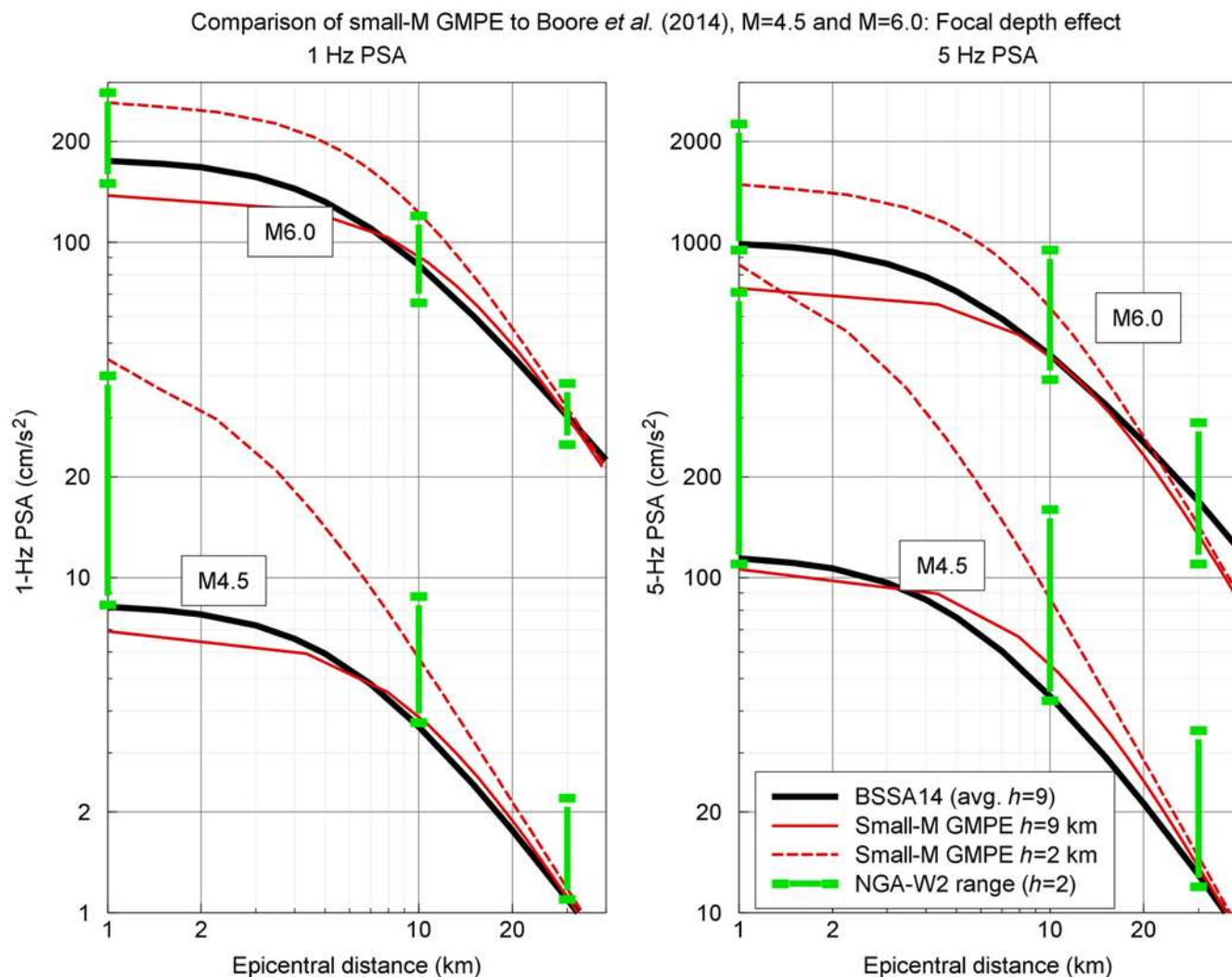
Figure 8. Effect of focal depth on predicted ground-motion amplitude for (left) 1 Hz and (right) 5 Hz PSA, in terms of surface distance (R_{JB} or epicentral distance). The thin solid line is the GMPE of this study, for an event of **M** 4.5 and **M** 6.0, with a focal depth of 9 km. The thick solid line shows the corresponding GMPE of Boore *et al.* (2014), which has an implied focal depth near 9 km. The dashed line shows corresponding PSA values from the GMPE of this study for a focal depth of 2 km. The range of amplitude estimates from the alternative NGA-West 2 GMPEs at epicentral distances of 1, 10, and 30 km for an event at 2 km depth (assuming that $R_{hypo} = R_{cd}$) is shown for each magnitude with solid vertical bars. The color version of this figure is available only in the electronic edition.

Campbell and Bozorgnia (2014) have a value of h_{eff} that is constant for all magnitudes, coupled with a magnitude-dependent attenuation; this gives their GMPE a shape that works well for the NGA-West 2 database overall but may not be optimal for small events at close distances (which are not well represented in the database). Idriss (2014) also has a fixed effective depth term (10 km). Boore *et al.* (2014) use a constant effective depth term that is determined by the regression (at each frequency; typically $h_{eff} \sim 5$ km). The Boore *et al.* (2014) form differs from the other NGA-West 2 models in its use of R_{JB} (distance to the surface projection of the rupture) as the distance metric. This is an advantage for some applications but may be a distinct disadvantage for induced-seismicity applications.

Overall, the NGA-West 2 models may provide a reasonable estimate of the amount of epistemic uncertainty, if the full range of estimates shown in Figure 8 is considered. One might argue that the uncertainty shown may be too broad on the low end of the range, as the distance–saturation effects for small shallow events are unlikely to be as large as those imposed by assuming that $h_{eff} = 9$ km. On the other hand, if the stress drop is lower for induced events than for natural earthquakes due to their shallow depths, then that would tend to lower their expected amplitudes, at least for higher frequencies, and would thus support a large uncertainty on the low side of the GMPE range. The GMPE of this study falls near the high end of the range of the NGA-West 2 models, being most similar to the Abrahamson *et al.* (2014) GMPE, at least at close distances.

In conclusion, the results of this study suggest that ground motions from small-to-moderate induced events could be significantly larger than would be predicted by most current

GMPEs (with the notable exception of that of Abrahamson *et al.*, 2014). This is due to their shallow focal depths, which bring the events very close to the epicenter. The nearness of the source may be partially mitigated, at least at high frequencies, by a tendency of shallow events to have lower stress parameters—but the resulting motions are still strong and potentially damaging. This study has provided a preliminary GMPE that describes the point-source scaling attributes of such events and may be used to assess their impact on seismic hazard. Further work with better datasets is required to fully understand the ground-motion and earthquake engineering implications of moderate events at close distances. Such studies need to address additional issues that are not resolved with the data analyzed here, including the distribution of stress parameters for induced events and their dependence on focal depth. Uncertainty in the stress parameter distribution for induced events implies significant uncertainty in their expected ground motions.

A limitation of the GMPE derived herein for seismic-hazard applications is that the simplicity of the selected functional form restricts its applicability to distances less than about 50 km. In equation (1), the attenuation term is modeled as linear in $\log R$, with no curvature in the slope due to growing anelastic effects at larger distances. This limitation is not important for the work provided here but could be inconvenient if the GMPE is to be plotted out to regional distances for purposes of comparisons with datasets over a wider distance range. For such purposes, a modification of equation (1) is needed. Specifically, we can introduce a nominal additional term $(+c_4 R)$ to force curvature of the attenuation line at regional distances without significantly impacting amplitudes at close distances:

$$\log Y = c_0 + c_1 \mathbf{M} + c_2 \mathbf{M}^2 + c \log R + c_4 R \qquad (4)$$

The coefficient c_4 is an effective anelastic attenuation coefficient chosen to have insignificant effect on amplitudes at <40 km but to provide curvature to the GMPE at larger distances. We can estimate an appropriate value for c_4, in consideration of the determined values for c_3, by comparing the amplitude decay provided by the GMPE of equation (1), when extrapolated to the 40–300 km distance range, to the decay provided over the same distance range by the NGA-West 2 GMPE of Boore *et al.* (2014) for small-to-moderate events. This comparison suggests a value of $c_4 = 0$ for $f \leq 1$ Hz; in other words, for low frequencies there is no additional anelastic effects that need be considered to extend the GMPE to regional distances. By inspection, the value of c_4 decreases linearly with log frequency from 1 to 10 Hz, attaining a minimum value of -0.002 that applies for $f \geq 10$ Hz. The value for PGA can be taken as that for 10 Hz PSA (-0.002), whereas the value of c_4 for PGV can be taken as that for 2 Hz PSA (-0.0006). This additional term should be applied if it is desirable to plot equation (1) to distances beyond 40 km, as might be required for comparison with data or other GMPEs, for example. The modified equation (equation 4) is not significantly different than equation (1) at low frequencies; at higher frequencies, it differs significantly only at larger distances.

For example, the maximum reduction in amplitudes relative to equation (1) (which is that resulting for 10 Hz amplitudes at 40 km) is 0.08 log units (about 20%). The added term becomes significant only at distances of ∼100 km and beyond. With this simple modification, the GMPE has an appropriate shape, in comparison with other GMPEs for California (such as the NGA-West 2 GMPEs), to distances of at least 300 km.

Data and Resources

The database of ground motions is the NGA-West 2 database (www.peer.berkeley.edu, last accessed May 2014), using the data selection criteria and site response corrections of Boore *et al.* (2014). Spectral amplitudes for the Douglas *et al.* (2013) database were provided by John Douglas and include data from the Koninklijk Nederlands Meteorologisch Instituut (Roswinkel and Voerendaal data), the International Centre for Geothermal Research (Hengill data; see Jousset *et al.*, 2011), Instituto Nazionale di Geofisica e Vulcanoogia (Camp Flegrei data), the Northern California Earthquake Data Center (Geysers data), the Swiss Seismological Service (Basel data), and Universite de Strasbourg (Soultz data). Simulations were performed using Stochastic-Method SIMulation (SMSIM), obtained from www.daveboore.com (last accessed June 2014). The work referred to as Yenier and Atkinson (2015) is a submitted manuscript entitled "A regionally-adjustable generic GMPE based on stochastic point-source simulations."

Acknowledgments

References

Abrahamson, N. A., W. J. Silva, and R. Kamai (2014). Summary of the Abrahamson, Silva, and Kamai NGA-West2 ground-motion relations for active crustal regions, *Earthq. Spectra* **30,** 1025–1056.

Allen, T., P. Cummins, T. Dhu, and J. Schneider (2007). Attenuation of ground-motion spectral amplitudes in southeastern Australia, *Bull. Seismol. Soc. Am.* **97,** 1279–1292.

Ancheta, T. D., R. B. Darragh, J. P. Stewart, E. Seyhan, W. J. Silva, B. S. J. Chiou, K. E. Wooddell, R. W. Graves, A. R. Kottke, D. M. Boore, T. Kishida, and J. L. Donahue (2014). PEER NGAWest2 database, *Earthq. Spectra* **30,** 989–1006.

Atkinson, G. (2014). Seismic hazard and ground motion implications of induced seismicity, *Seismol. Res. Lett.* **85,** 464.

Atkinson, G., and D. Boore (2006). Ground motion prediction equations for earthquakes in eastern North America, *Bull. Seismol. Soc. Am.* **96,** 2181–2205.

Atkinson, G., and D. Boore (2014). The attenuation of Fourier amplitudes for rock sites in eastern North America, *Bull. Seismol. Soc. Am.* **104,** 513–528.

Atkinson, G., and T. Hanks (1995). A high-frequency magnitude scale, *Bull. Seismol. Soc. Am.* **85,** 825–833.

Atkinson, G. M., and M. Morrison (2009). Observations on regional variability in ground-motion amplitudes or small-to-moderate earthquakes along the west coast of North America, *Bull. Seismol. Soc. Am.* **99,** 2393–2409.

Atkinson, G., and W. Silva (2000). Stochastic modeling of California ground motions, *Bull. Seismol. Soc. Am.* **90,** 255–274.

Atkinson, G., D. W. Greig, and E. Yenier (2014). Estimation of moment magnitude ($\mathbf{M}$) for small events ($\mathbf{M} < 4$) on local networks, *Seismol. Res. Lett.* **85,** 1116–1124.

Babaie Mahani, A., and G. Atkinson (2013). Regional differences in ground-motion amplitudes of small-to-moderate earthquakes across North America, *Bull. Seismol. Soc. Am.* **103,** 2604–2620.

Boore, D. M. (2000). SMSIM; Fortran programs for simulating ground motions from earthquakes, v. 2.0, *U.S. Geol. Surv. Open-File Rept. 00-0509*, 55 pp., available from www.daveboore.com; last accessed June 2014.

Boore, D. M. (2003). Prediction of ground motion using the stochastic method, *Pure Appl. Geophys.* **160,** 635–676.

Boore, D. M. (2009). Comparing stochastic point-source and finite-source ground-motion simulations: SMSIM and EXSIM, *Bull. Seismol. Soc. Am.* **99,** 3202–3216.

Boore, D. M., J. Stewart, E. Seyhan, and G. Atkinson (2014). NGA-West2 equations for predicting response spectral accelerations for shallow crustal earthquakes, *Earthq. Spectra* **30,** 1057–1086.

Campbell, K. W., and Y. Bozorgnia (2014). Campbell–Bozorgnia NGA-West2 ground motion model for the average horizontal components of PGA, PGV, and 5%-damped linear response spectra, *Earthq. Spectra* **30,** 1087–1116.

Chiou, B. S. J., and R. Youngs (2014). Update of the Chiou and Youngs NGA ground motion model for average horizontal component of peak ground motion and response spectra, *Earthq. Spectra* **30,** 1117–1154.

Douglas, J., B. Edwards, V. Convertito, N. Sharma, A. Tramelli, D. Kraaijpoel, B. Cabrera, N. Maercklin, and C. Troise (2013). Predicting ground motion from induced earthquakes in geothermal areas, *Bull. Seismol. Soc. Am.* **103,** 1875–1897.

Ellsworth, W. (2013). Injection-induced earthquakes, *Science* **341,** no. 6142, doi: 10.1126/science.1225942.

Frolich, C., W. Ellsworth, W. Brown, M. Brunt, L. Luetgert, T. MacDonald, and S. Walter (2014). The 17 May 2012 *M* 4.8 earthquake near Timpson, East Texas: An event possibly triggered by fluid injection, *J. Geophys. Res.* **119,** 581–593.

Idriss, I. (2014). An NGA-West2 empirical model for estimating the horizontal spectral values generated by shallow crustal earthquakes, *Earthq. Spectra* **30,** 1155–1178.

Jousset, P., C. Haberland, K. Bauer, and K. Arnason (2011). Hengill geothermal volcanic complex (Iceland) characterized by integrated geophysical observations, *Geothermics* **40,** 1–24.

Joyner, W., and D. Boore (1993). Methods for regression analysis of strong motion data, *Bull. Seismol. Soc. Am.* **83,** 469–487.

Keranen, K., H. Savage, G. Abers, and E. Cochran (2013). Potential induced earthquakes in Oklahoma, USA: Links between wastewater injection and the 2011 M_w 5.7 earthquake sequence, *Geology* **41,** 699, doi: 10.1130/G34045.1.

Raoof, M., R. Herrmann, and L. Malagnini (1999). Attenuation and excitation of three-component ground motion in sourthern California, *Bull. Seismol. Soc. Am.* **89,** 888–902.

Rubinstein, J. (2014). Quantifying the seismic hazard from natural and induced earthquakes, *Seismol. Res. Lett.* **85,** 464.

Sumy, D., E. Cochran, K. Keranen, M. Wei, and G. Abers (2014). Observations of static Coulomb stress triggering of the November 2011 *M* 5.7 Oklahoma earthquake sequence, *J. Geophys. Res.* **119,** doi: 10.1002/2013JB010612.

Worden, B., M. Gerstenberger, D. Rhoades, and D. Wald (2012). Probabilistic relationships between ground motion parameters and modified Mercalli intensity in California, *Bull. Seismol. Soc. Am.* **102,** 204–221.

Yenier, E., and G. Atkinson (2014). Point-source modeling of moderate-to-large magnitude earthquakes and associated ground-motion saturation effects, *Bull. Seismol. Soc. Am.* **104,** 1458–1478.

Department of Earth Sciences
Western University
London, Canada N6A 5B7
gmatkinson@aol.com